# Supplementary figures for Han and Deng *et al.*, Immune microenvironment subtypes and association with tumor cell mutations and antigen expression in follicular lymphoma

Contents

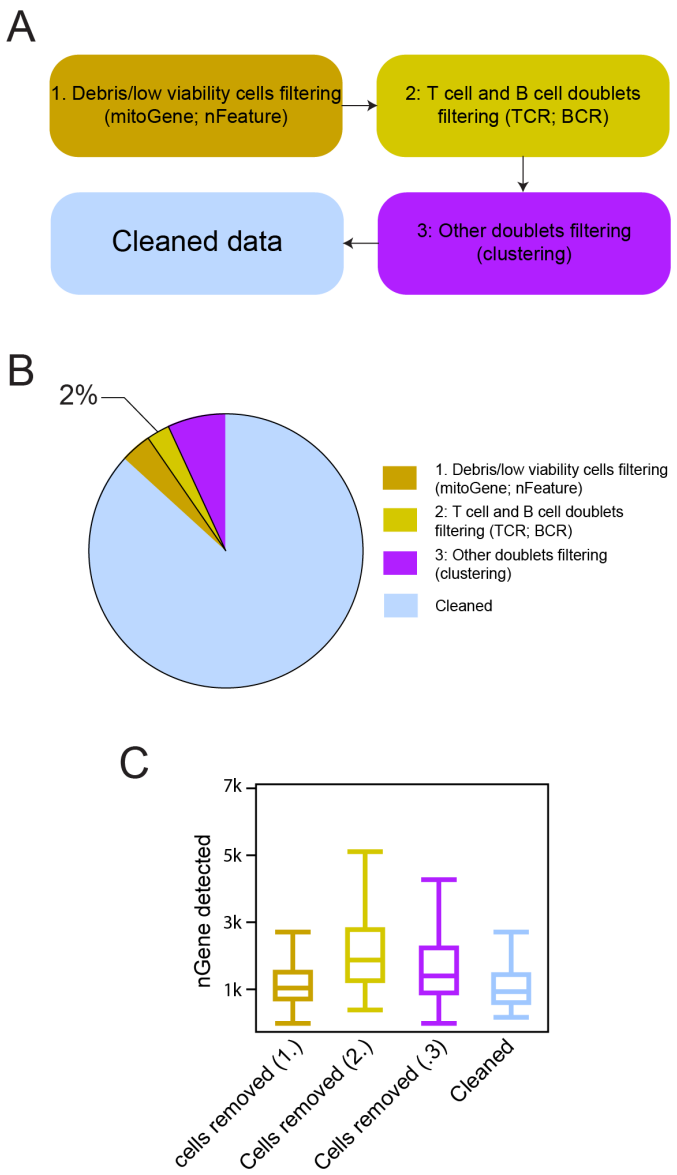


**Figure S1. Quality filtering of cells.** The schema showing quality filtering steps applied to cells (A), the piechart showing the fraction of cells specific to each step averaged across samples (B) and the boxplot showing the number of genes detected for cells involved in each step (C). The doublets removed in step 2 had on average nearly twice more transcripts detected per cell compared to the cleaned singlets, which is consistent with the characteristics of doublets.

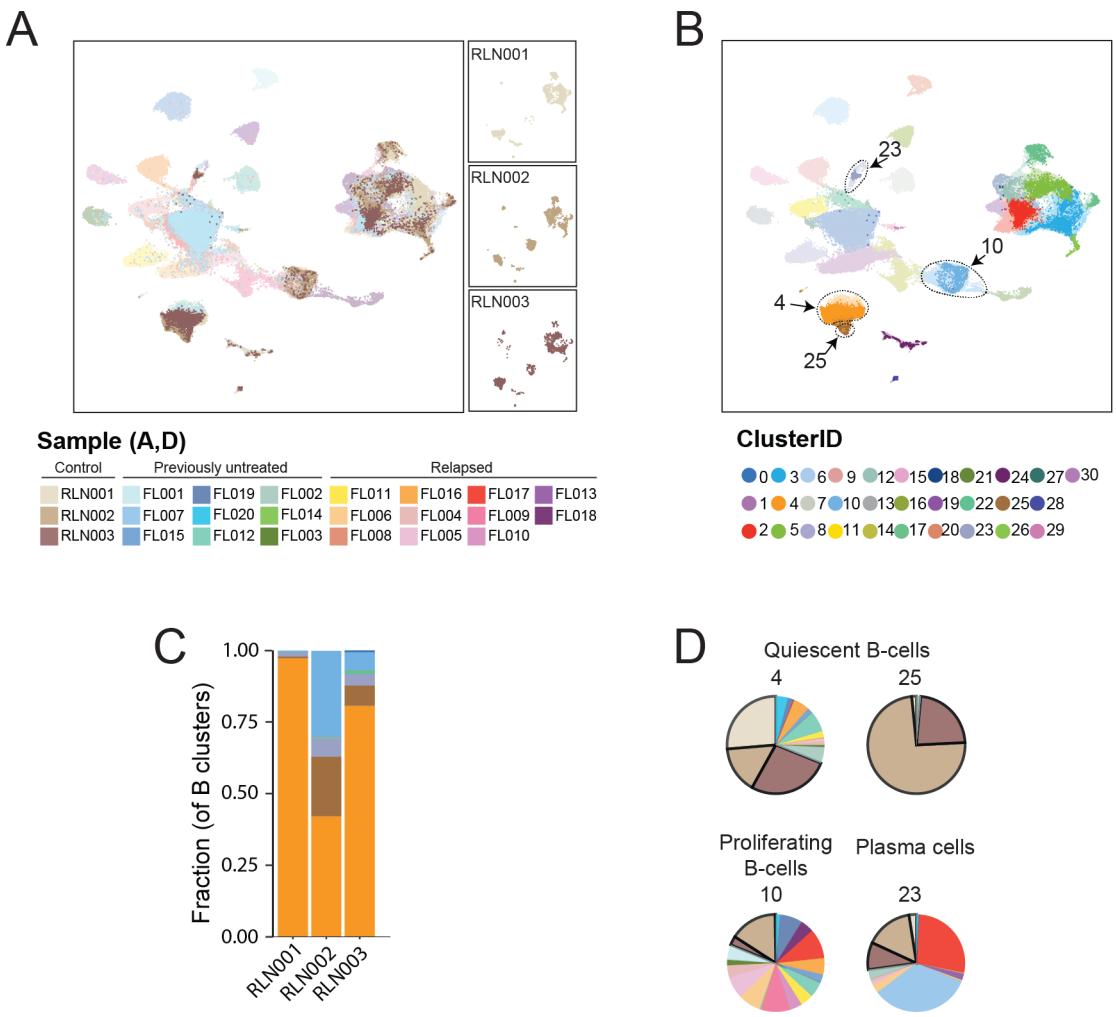


**Figure S2. Cluster distribution of cells from reactive lymphoid nodes (RLN). A,** The UMAP visualization of all cells colored by sample ID (left) and the sample UMAP visualization showing cells from 3 RLN samples (right), corresponding to Figure 1A and 1B. **B,** UMAP visualization of B cells showing clusters that contain B cells from RLN samples, corresponding to Figure 1A and 1B. **C**, Barplot showing cell composition by cluster ID across RLN samples. **D**, Pie charts showing cell composition by sample ID in quiescent B-cells, proliferating B cells and plasma cells.

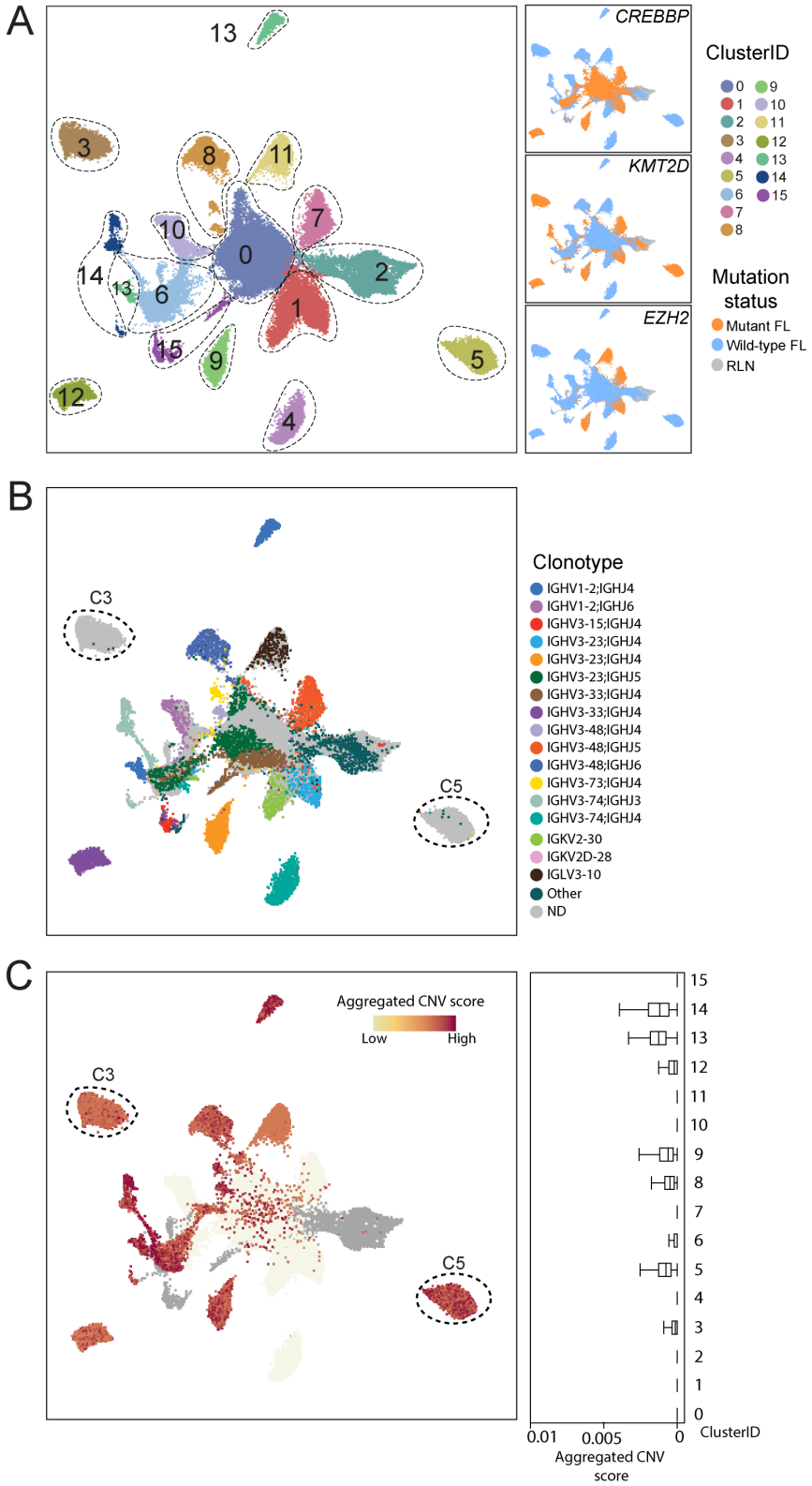


**Figure S3. UMAP visualizations of B cells from all patients.** The UMAP visualization of B cells are colored by cluster ID (A, left), driver gene mutation (A, right), the clonotypes defined with Single cell V(D)J sequencing (B), and the aggregated copy number variation (CNV) scores (C).

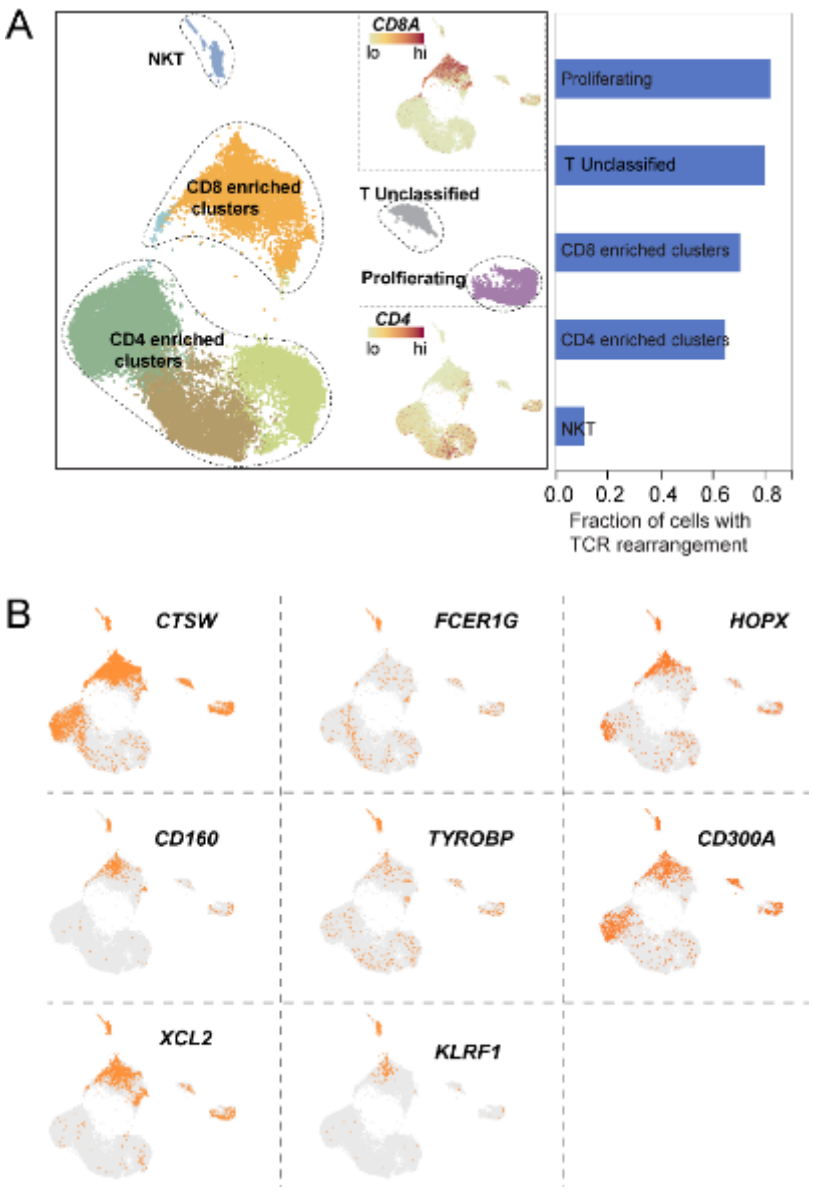


**Figure S4. Unsupervised sub-clustering of T and NK cells from all patients. A,** UMAP visualization of T cells and NK cells from all patients colored by cluster ID (left) and the barplot showing fraction of cells with detectable TCR rearrangement per cell type based on scTCR-seq (right). Feature plots of CD8A and CD4 are shown in insets at top right and bottom right, respectively. Lo, low expression; hi, high expression. **B,** Feature plots of representative genes. Orange colored cells denotes the corresponding gene expression level (logUMI) > 0.

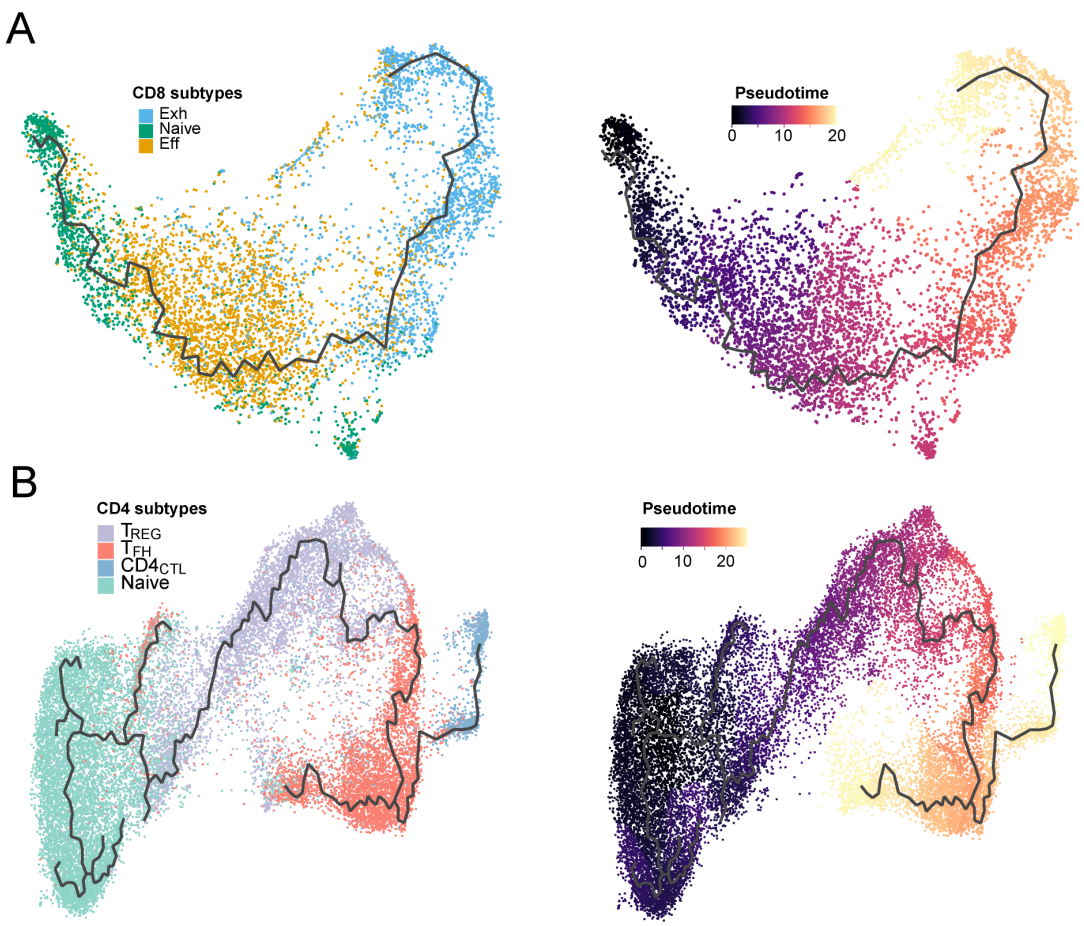


**Figure S5. Potential developmental trajectories for CD4 T-cells and CD8 T-cells from all patients inferred by Monocle 3 analysis. A**, Monocle trajectory plots showing cells colored by CD8 T-cell subpopulations (left) and by inferred pseudotime (right). **B,** Monocle trajectory plots showing cells colored by CD4 T-cell subpopulations (left) and by inferred pseudotime based on global expression profiles (right).

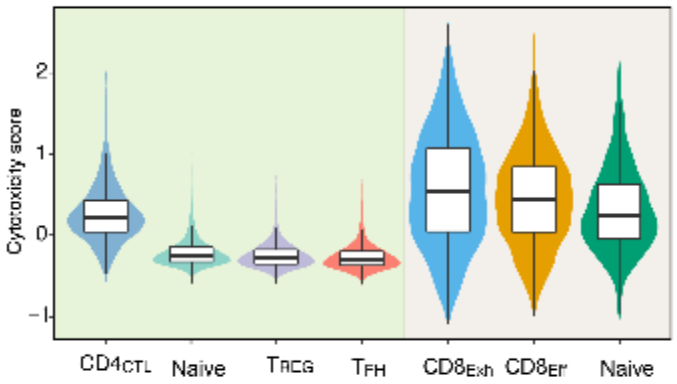


**Figure S6. Cytotoxicity signature scores of CD4 and CD8 T-cell populations.** Violin plots show the level of cytotoxic signature score across CD4 and CD8 T-cell populations.

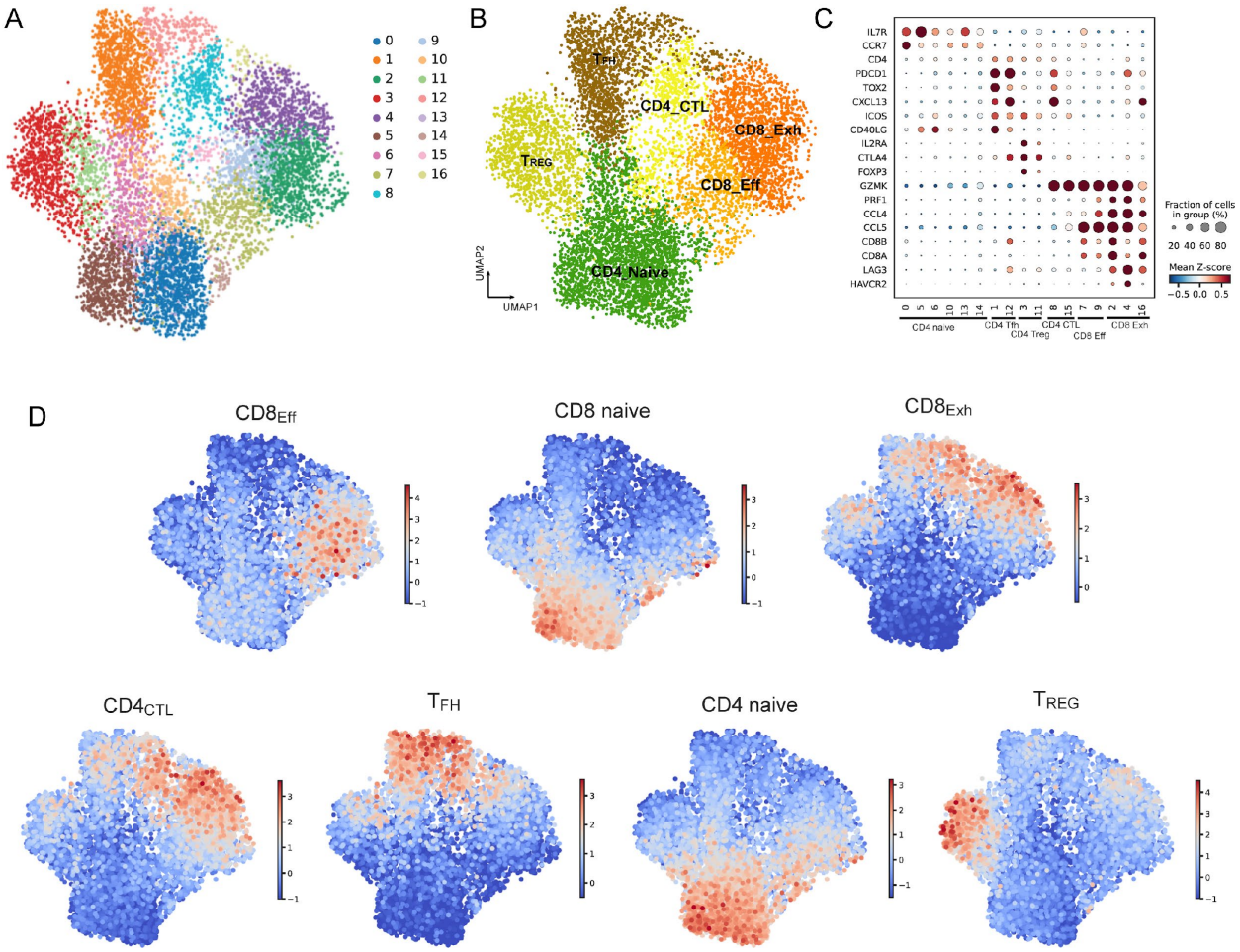


**Figure S7. Independent cohort validation of CD4 and CD8 T cells subpopulations. A,** UMAP visualization of T-cells colored by cluster ID from the independent cohort from Roider et al. (8,453 cells) using L. **B**, UMAP visualization colored by assigned cell types. **C**, Bubble plot showing the fraction of cells expressing signature genes (indicated by the size of the circle) as well as their scaled expression levels (indicated by the color of the circle), highlighting high GZMK expression in an independently validated cytotoxic CD4 T-cell population. **D,** UMAP plots show the GSVA scores of cluster marker genes from CD4 and CD8 T-cell populations in Figure 2B and 2D projected over the independently-defined clusters from Roider *et al.* Despite fewer cells (8,453 T-cells) compared to this study (29,482 T-cells), projection of signature genes from the clusters defined in our CD4 and CD8 T-cell populations largely agree with the independently defined clusters from Roider et al.. Overlap is noted for CD8Exh and CD4CTL GSVA scores, likely due to the relatively lower sequencing depth in the Roider *et al.* study compared to this study and the overlap of highly-expressed signature genes such as GZMK.

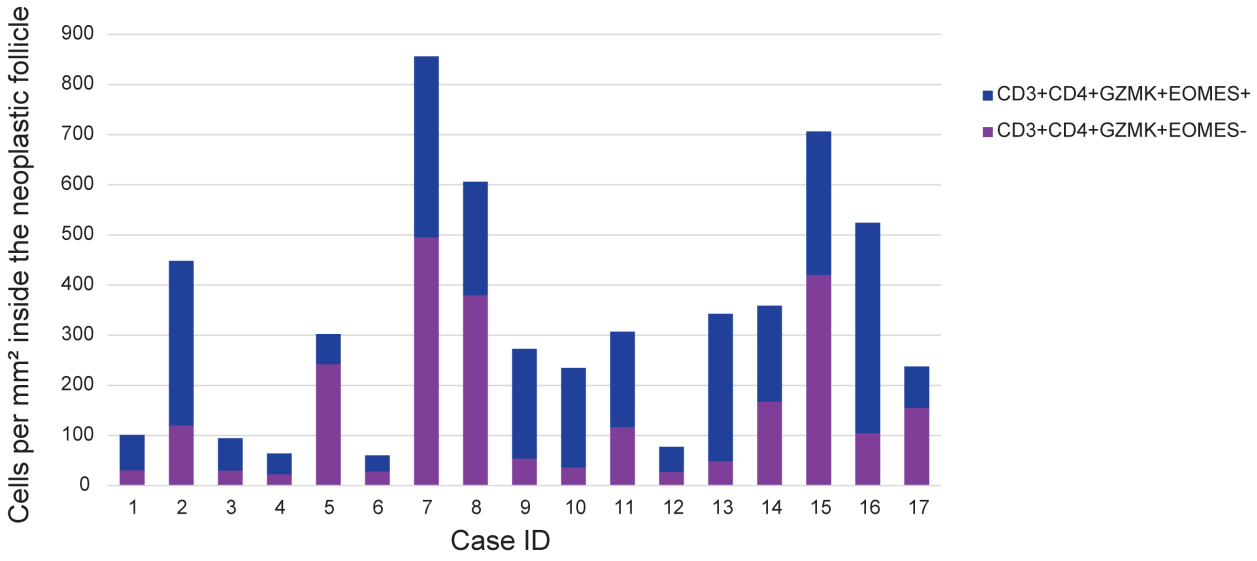


**Figure S8: Densities of cytotoxic CD4 T-cells within the neoplastic follicles of FL tumors measured by multiplexed immunofluorescence imaging.**

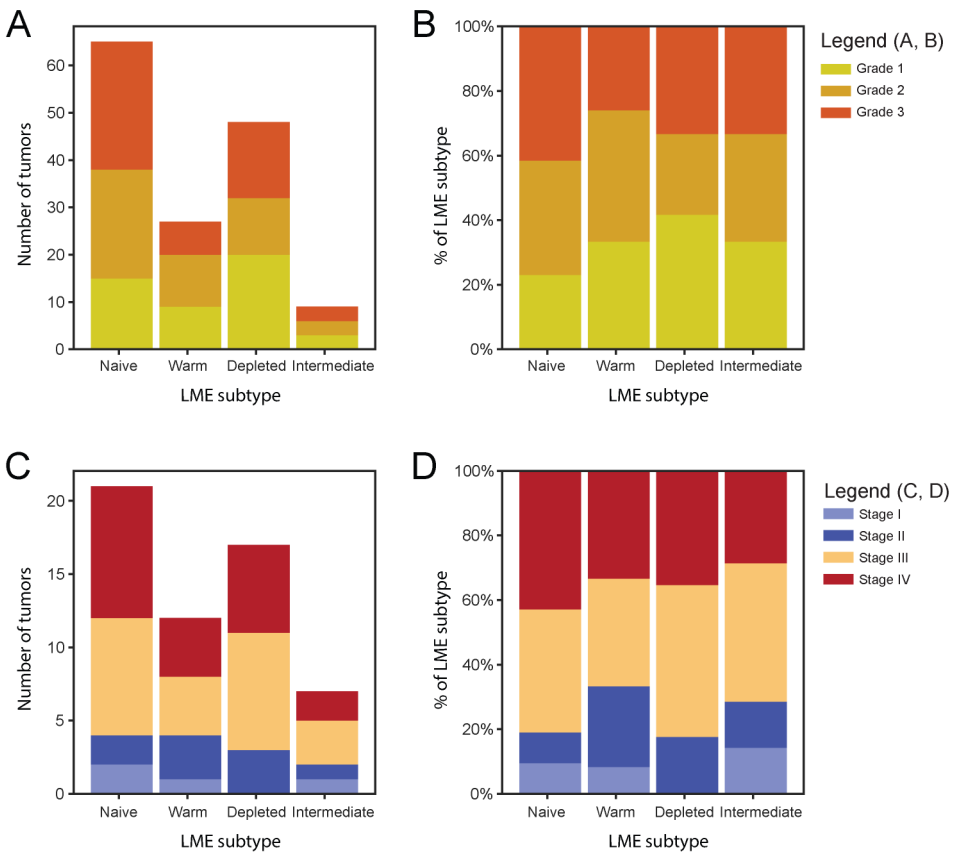


**Figure S9. Association between LME subtypes and tumor grade and stage.** The stacked barplots showing absolute number of tumors colored by grade across LME subtypes (A) and the relative fraction of tumors colored by grade across LME subtypes (B). The stacked barplots showing absolute number of tumors colored by stage across LME subtypes (C) and the relative fraction of tumors colored by stage across LME subtypes (D).

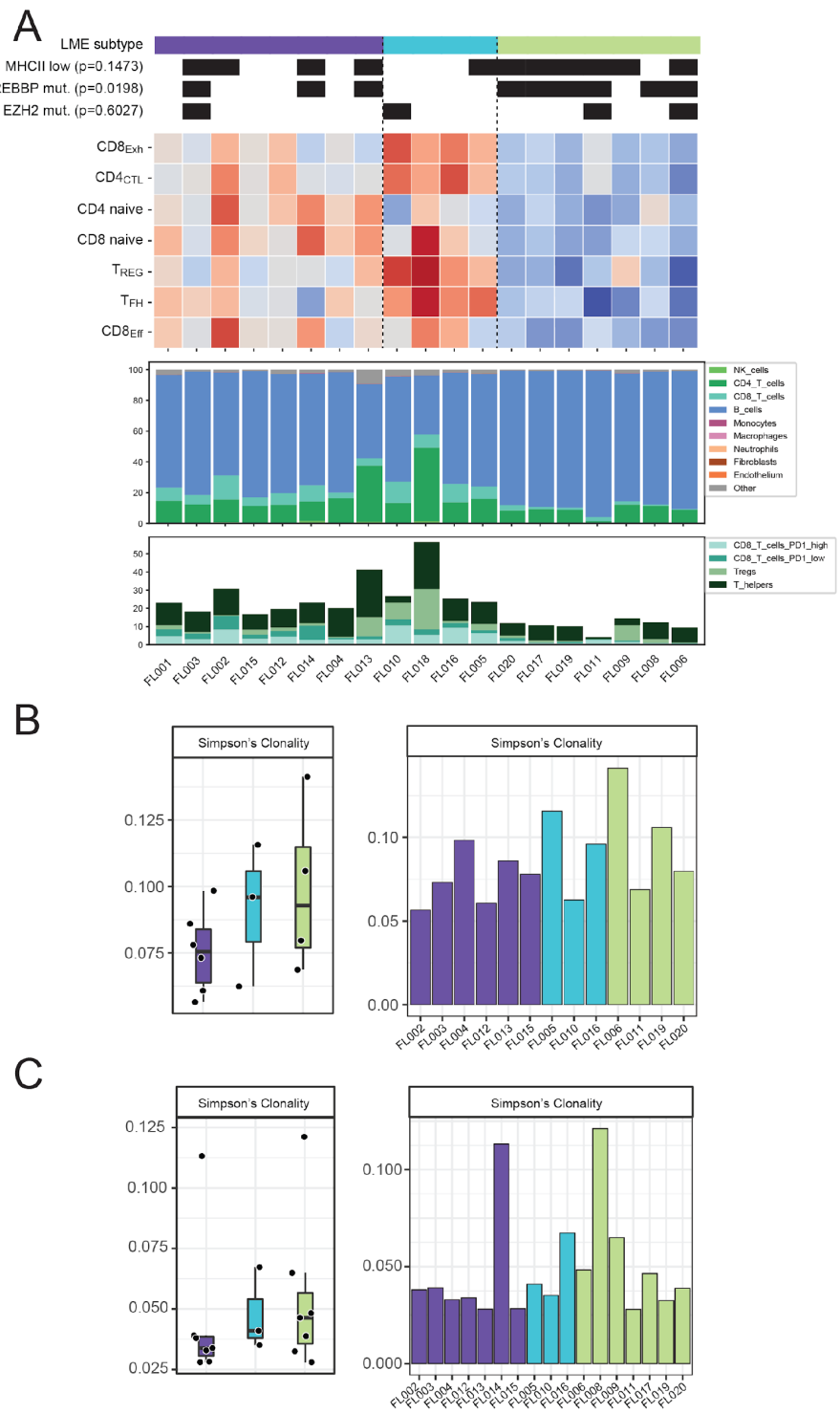


**Figure S10: Deconvolution of pseudobulk transcriptomes from scRNA-seq dataset into LME subtypes. A,** Heatmap showing the relative abundancy of CD8 and CD4 T-cell populations based on the deconvolution of pseudobulk transcriptomes (A). Three sample level annotations including driver gene mutation status of *CREBBP* and *EZH2* as well as the MHCII expression status were labelled as black bars above the heatmap. P values within the parentheses of the

annotations denote the significance level of association between the corresponding annotation and the LME subtype. P values were calculated by using two-tailed fisher exact tests. **B-C,** Simpson's clonality scores are shown for CD4 (B) and CD8 (C) with available samples, colored according to LME subtype as in A.

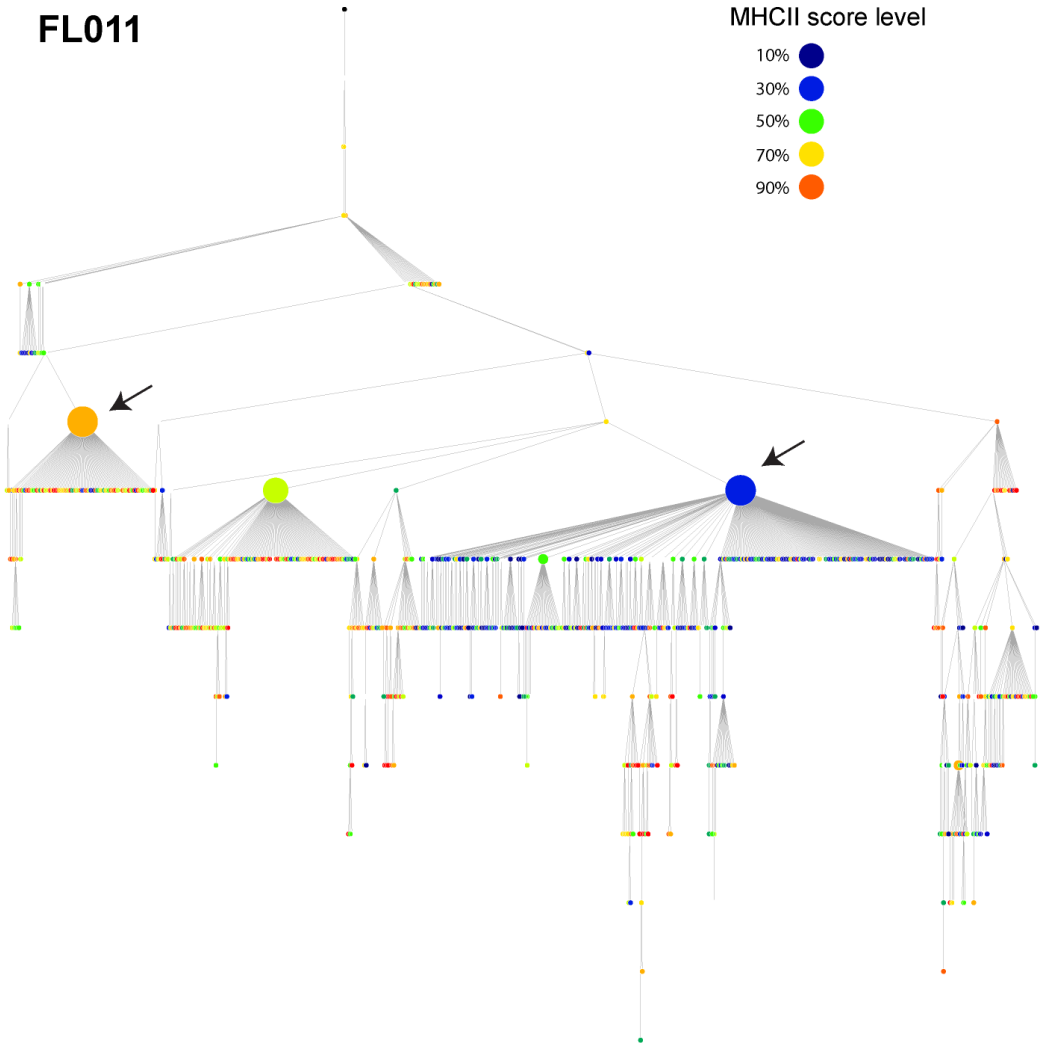


**Figure S11. Correlation between MHCII expression scores and the immunoglobin hierarchy.** The immunoglobulin hierarchy tree was reconstructed using all malignant B cells of a MHC-II-high patient (FL-011) and the MHCII scores was defined using the differentially expressed MHC II genes identified in this study.

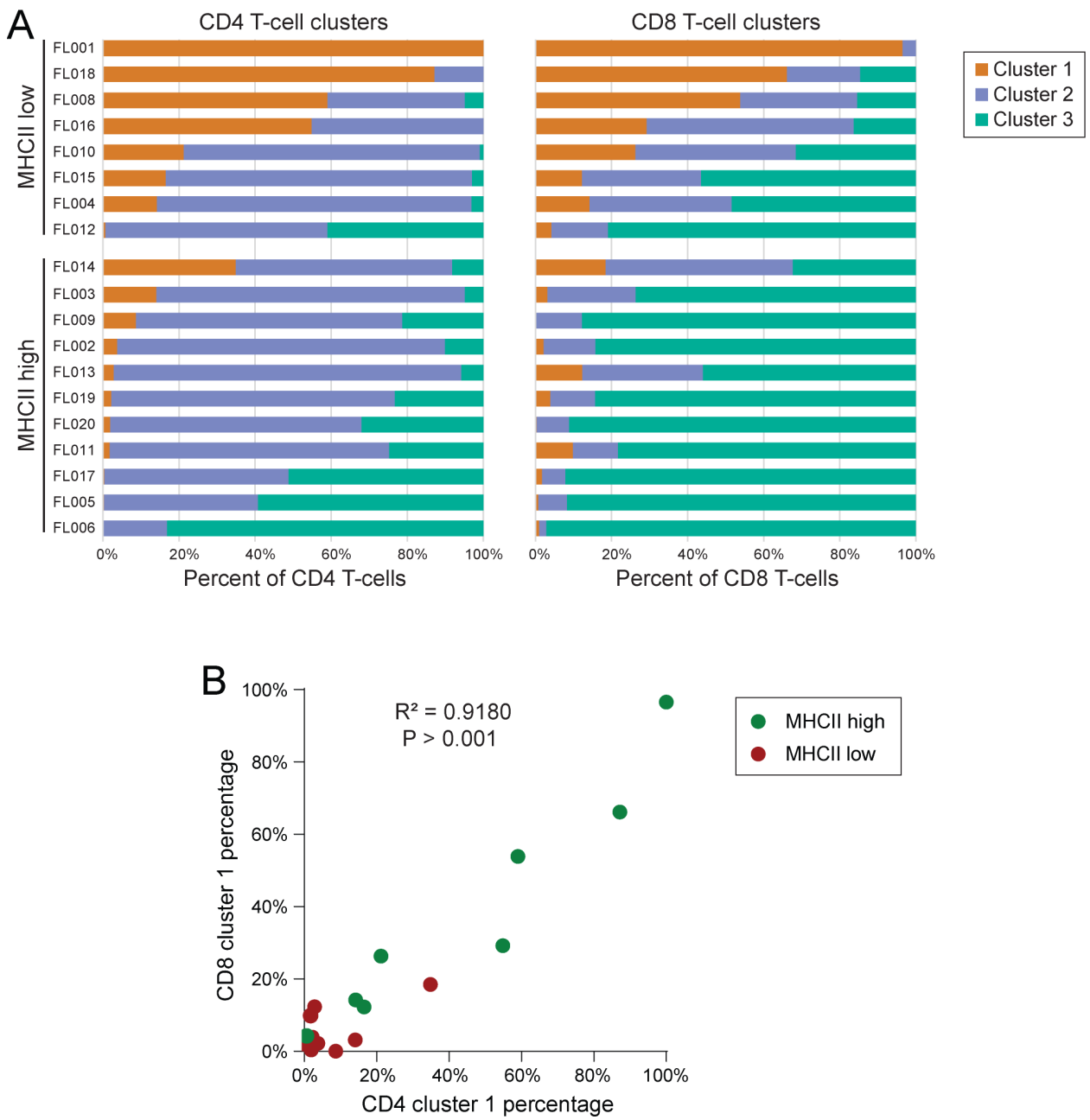


**Figure S12: Sample distribution across clusters in Figures 4E and 4H. A,** The proportion of CD4 (left, clusters corresponding to figure 4H) and CD8 (right, clusters corresponding to figure 4E) T-cells falling within each DEG cluster are shown for MHCII low and (above) and MHCII high (below) tumors. B, Correlation between the fractions of CD8 cells within cluster 1 (corresponding to figure 4E) and that of CD4 cells within cluster 1 (corresponding to figure 4H) is shown. Correlation was tested using Pearson's correlation.